Chemistry and Materials Research
ISSN 2224- 3224 (Print) ISSN 2225- 0956 (Online)
Vol.6 No.4, 2014
www.iiste.org

Influence of Preparation Method on Copper Loaded Titania Nanoparticles: Textural, Structural Properties and Its Photocatalytic Activity towards P-Nitrophenol

Radwa Elsalamony*, Dalia Abd El-Hafiza

Egyptian petroleum Research Institute, PO box 11727, Cairo, Egypt

* E-mail of the corresponding author: radwa2005@hotmail.com

Abstract

TiO_2 nanopowder, loaded with copper, was prepared under both impregnation and co-precipitation methods. The morphology and structure of TiO_2 were studied by XRD, TEM, FTIR and BET techniques. The photocatalytic activity of samples was studied by monitoring the degradation of nitro phenol, using a UV-visible spectrophotometer. Total organic compound measurements showed that p-nitrophenol photodegradation efficiency reached 46% after 150 min over Cu-TiO_2 catalysts.

Key words: TiO_2 nanopowder, copper, impregnation, co-preceptation, photodegradation, nitrophenol.

1. Introduction

p-Nitrophenol (PNP) is one of the most hazardous refractory pollutants with high stability and solubility in water. It can be found in industrial and agricultural wastewaters, posing a significant environmental and public risk. Generally, these PNP molecules can be effectively decomposed by several advanced oxidation processes (AOPs), for example, microwave-assisted oxidation (Bo *et al.* 2006), electro-catalytic oxidation (Quiroz *et al.* 2005), radiation-induced catalytic oxidation (Yu *et al.* 2010), and photoelectrocatalytic oxidation (Su et al. 2009). However, the requirements of various devices, the complex designs of oxidation systems, or low degradation efficiency limit the practical applications of these methods. Photoinduced oxidation, which is also an AOP, is economical, environmentally friendly, and promising in treating contaminated water.
Photocatalysis has been widely used for the abatement of organic and inorganic pollutants. TiO_2 is the most common photocatalyst because of it is optical and electronic properties, low cost, chemical stability and non-toxicity (Pelizzetti & Serpone 1986; Schiavello 1988; Pelizzetti & Serpone 1989).

However, its photocatalytic efficiency can be limited by stabilization of the charge photocarriers in the bulk of the material, by fast electron–hole recombination either at the bulk or at the surface of the oxide or by its relatively large band gap which limits light absorption in the visible region (Malato *et al.* 2009; Augugliaro *et al.* 2006; Anpo & Tackeuchi 2003).

Among strategies aimed at reducing electron–hole recombination rates and to decrease simultaneously the band gap of the material, it is common to employ methods based on doping the titania catalyst with transition metal cations while maintaining a good control of the primary particle size to achieve nanoscale configurations of the catalysts (Khann & Shetty 2014; Farbod & Kajbafvala 2013).
In general terms, it appears that optimum photocatalytic properties can be achieved upon doping at a relatively weak level (Adán et al. 2007; Litter & Navío 1996), which can be closely related to the dynamics of the recombination process, in turn linked to the distance between dopant cations in the titania lattice (Litter & Navío 1996).
Recently, Cu_2O, as a new type of photocatalyst, has attracted much attention because it has low toxicity, is environmentally friendly, and has a narrow direct band gap (2.17 e.V) that can be easily activated by visible light. In many studies, Cu_2O can be efficiently used in the photocatalytic degradation of various

dyes and in the decomposition of water into H_2 and O_2 (Kuo & Huang 2008; Somasundaram *et al.* 2007); when Cu_2O particles alone were used directly (Cao *et al.* 2010), the degradation process took longer to obtain a low efficiency. In addition, Cu_2O particles cannot be immobilized and have to be directly dispersed in solutions, which inevitably results in the aggregation of different particles, a decrease in the activities, and make the particles difficult to recycle. In photodegradation of PNP and other organic pollutants, only Cu_2O/TiO_2 (Chen *et al.* 2013) doped TiO_2 (Khalid *et al.* 2013) and Copper phthalocyanine tetrasulfonate-modified TiO_2 ($CuPcTs/TiO_2$) nanoparticles (Zhiyu et al. 2006) have ever been reported exhibiting high efficiency.

The loading ions that are considered as dopants are usually confined as much dispersed species onto the surface and/or as a few top layers of TiO_2 particles. This is due to the moderate calcination temperatures used in the conventional preparations. A comparison among the results reported in the literature for doped TiO_2 samples is difficult since the preparation methods of the photocatalysts are usually different (Palmisano et al. 1997). It would be necessary to use the same bare TiO_2 as the starting material by scrutinizing carefully the various insights deriving from the characterization results.

In this paper it is reported a study on the physicochemical characterisation and photocatalytic activity of high surface area nanoTiO_2 powders prepared by gamma irradiation loaded with copper ions. The samples were prepared by using the wet impregnation and co-precipitation methods. The solids were characterized by X-ray diffraction (XRD), specific surface area (BET) and porosity determination, transmission electron microscopy (TEM), and Fourier transform infrared spectroscopy (FTIR). The results have been used in order to correlate the properties of the powders with their photocatalytic activity for the photodegradation of p-nitrophenol and the photoreactivity results were compared with those obtained when a pure prepared TiO_2 sample were used.

2. Experimental

2.1 Preparation method

$Ti(OH)_4$ gel was obtained at room temperature by the addition of concentrated ammonia solution (35% NH_3) dropwise to a vigorously stirred dilute solution of $TiCl_4$ (Fluka, 15%) until a pH 9 was attained. The ammonia solution was added dropwise to prevent particle adhesion and sudden grain growth of particles. The white hydrous $Ti(OH)_4$ solution was irradiated under a ^{60}Co source (NCRRT) with 30 kGy and at a dose rate of 3.3476 kGy/h. The reactant solution was stirred mildly while irradiating it, so as not to become agglomerated with each other. The particles were then washed rigorously and repeatedly with bidistilled water to remove any remaining impurities. After the solvent was evaporated at 100 °C for 24 h, the precipitates were dried at 300 °C for 2 h to remove NH_4Cl, and then calcined at 500 °C for 4 h to get titania TiO_2. A 0.5% Cu/TiO_2 was prepared by an impregnation the TiO_2 carrier using copper nitrate $Cu(NO_3).6H_2O$ as a precursor for copper metal. A third sample 0.5% $Cu\text{-}TiO_2$ was prepared by a sol-gel method. Cu-doped TiO_2 nanoparticles containing 0.5wt% Cu (II) ion dopant were synthesized via a co-precipitation. Briefly, 6 mL ethanol solution of 0.5 M of $Cu(NO_3).6H_2O$ was added dropwise to $TiCl_4$ solution under stirrering. The pH value of the reaction solution was adjusted to ca. 9 by ammonia. Then the pale blue and dense colloid was formed. The colloid was stirred gently for 3h, and then washed rigorously and repeatedly with bidistilled water to remove any remaining impurities. After the solvent was evaporated at 100 °C for 24 h, the precipitates were dried at 300 °C for 2 h to remove NH_4Cl, and then calcined in an air stream of 400 °C for 4 h.

2.2 Experimental procedure

The photoreactor was designed by us. The light source was a 254 nm UV lamp. A general photocatalytic procedure was carried out as follows: nitrophenol was chosen as the model molecule; 1g/L of the catalyst was suspended in the nitrophenol solution (C_0 (NP) = 10, 20, 30, 40, 50 ppm), natural PH, $V_{solution}$ = 300ml and the suspension were irradiated with UV lamp open to air. During the process of the photocatalytic tests, the concentration of nitrophenol was detected using a visible spectrophotometer (JENWAY-6505) at λ_{max} 458 nm.

2.3 Physical characterization of the catalysts

N_2 physisorption studies were carried out in a NOVA Automated gas sorption system Version 1.12. For each measurement, the sample was degassed at 250 ^oC for 3–4 h, and then analyzed at 77 K (liquid N_2 temperature). The surface areas and pore volumes were determined using the BET (Brunauer–Emmett–Teller) method from the adsorption branch in the relative pressure range of 0.05-0.35. The total pore volume of the samples was calculated from the nitrogen uptake at $P/P_o = 0.95$, using the BJH (Barrett–Joyner– Halenda) method from the isothermal desorption data. The geometrical specific surface area (S_{XRD}) was also determined, assuming spherical particles, according to Equation (1) (Dobrosz-Gómeza *et al.* 2012; Fuentes *et al.* 2010):

$$S_{XRD} = \frac{6\ x\ 10^3}{\rho\ D_{XRD}} \qquad (1)$$

where, ρ (g cm^{-3}) is the theoretical density calculated from $\rho = \frac{n\ M_r}{V_c\ x\ N_c}$, n is atoms per unit cell, M_r is molecular weight in gm/mol, V_c is volume per unit cell (cm^3) and N_A is Avogadro's number (6.022 x 10^{23}) and D_{XRD} (nm) is the particle size, according to the Scherrer formula.

XRD analysis was performed to determine the rutile and anatase concentrations. X-ray powder diffraction (XRD) patterns were obtained with a PANalytical X'Pert PRO diffractometer in reflection mode using Cu Kα radiation over the scan range of 2θ between 20 and 80 at 295 K, in order to identify the phase present.

Crystallite size (D_{XRD}) of the photocatalysts was calculated from the line broadening of X-ray diffraction peak according to the Sherrer formula [10], as shown in Equation (2):

$$D_{XRD} = \frac{K\lambda}{\beta\ cos(\theta)} \qquad (2)$$

where *K* is the Sherrer constant (0.89), λ is the wavelength of the X-ray radiation (0.15418 nm for Cu K_α), β is the full width at half maximum (FWHM) of the diffraction peak measured at 2θ, and θ is the diffraction angle. The geometrical mean particle size (D_{BET}) was also calculated using BET data, assuming spherical particles, according to Equation (3) (Dobrosz-Gómeza *et al.* 2012; Fuentes *et al.* 2010):

$$D_{BET} = \frac{6\ x\ 10^3}{\rho\ S_{BET}} \qquad (3)$$

where ρ (g cm^{-3}) is the theoretical density, and S_{BET} (m^2g^{-1}) is the measured S_{BET}.

Total amount of acidity was estimated from weight loss measurements of adsorbed pyridine using SETARAM Labsys TG-DSC16 equipment. After that, the samples were analyzed by TGA.

FTIR were performed using Nicolet Is-10 model (USA) Infrared spectrophotometer adopting KBr technique. For all samples, the KBr technique was carried out approximately in a quantitative manner since the weight of sample and that of KBr, were always kept constant.

The topography and particle size of TiO_2 was measured using JEOL transmission electron microscopy (TEM) operating at an accelerating voltage of 120 Kv. The structure resolution of microscope is 0.2 nm. Prior to the analysis, the catalyst sample was ground into powder (using mortar and pestle) and then ultrasonically dispersed in water and placed on a carbon-coated copper grid. The sample was allowed to dry before TEM analysis.

The total organic carbon (TOC) of the 4-NP solutions was analyzed using an Analytik Jena, multi N/C 2100 S; HT 1300 (made in Germany) to evaluate the mineralization degree of the organic material.

3. Results and discussion

3.1 Characterization results of photocatalysts

3.1.1 N2 adsorption–desorption results

In order to verify the mesoporosity of the photocatalyst samples, the N_2 adsorption–desorption analysis is very powerful technique normally used. The N_2 adsorption–desorption isotherms of the synthesized TiO_2 exhibits typical IUPAC type IV pattern as shown in Figure 1. TiO_2 tends to give Type H2 loops, often referred to as 'ink bottle' pores. Whereas; Cu-TiO_2 catalyst show H3 hysteresis loop, it does not exhibit any limiting adsorption at high P/P_o values. It is often observed with aggregates of plate-like particles giving rise to slit-shaped pores.

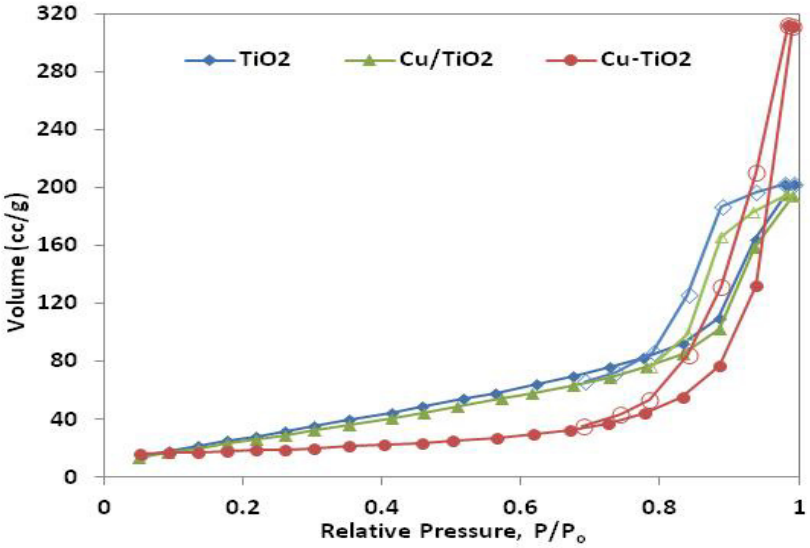

Figure1. N_2 Adsorption-Desorption isotherm of TiO_2

A hysteresis loop in the isotherms was observed with dissimilar shapes for the adsorption and desorption branches, implying a different size of pore throat diameter. The sharp drop on the desorption branch can be assigned to the presence of mesopore constrictions at the boundaries between the ordered domains and of smaller pores in the titania walls [24]. The Barrett, Joyner and Halenda (BJH) pore diameters measured from the adsorption and desorption branches were 15.27 nm and 11.50 nm, respectively for Cu-TiO_2 catalyst. These results imply good homogeneity of the pores. The main structural characteristics deduced from the isotherms and the comparison between experimental (specific surface area: S_{BET}; mean particle size: D_{XRD}) and geometrical data (S_{XRD}, D_{BET}) are reported in Table 1.

Table 1. Textural and structural properties of TiO_2 Catalysts

Samples	D_{XRD}[a] (nm)	D_{BET} (nm)	Agglomeration Ratio	D_{BJH} (nm)		S_{BET}[b] (m^2/g)	S_{XRD} (m^2/g)	Pore Radius Dv(r)[c] (nm)	Total pore Volume[c] (cc/g)	Acidity µmol/gm
				Ads.	Des.					
TiO_2	22.35	60.5	0.034	2.47	11.61	127.1	343.8	1.24	0.334	6055
Cu/TiO_2	16.91	33.2	0.023	2.25	15.83	115.8	227.7	1.13	0.324	6334
Cu-TiO_2	18.62	63.3	0.021	15.27	11.50	60.8	206.8	1.01	0.476	13343

[a] according to XRD analysis.

[b]BET surface area calculated from the linear portion of the BET plot in the relative pressure range of $p/p_0 = 0.05–0.35$.

[c] Pore radius and total pore volume estimated using BJH method from the isothermal desorption data.

When using the Scherer equation, we assume that the particle size effects are only peak broadening; however, if the particles are non-uniform, the particle size will be underestimated. The mean particle size (D_{BET}) can be obtained from the BET data assuming that the particles are spherical. The calculated D_{BET} values are always bigger than those of the D_{XRD}. This deviation can be explained by a potential presence of small agglomerates and grain in the boundary interfaces of catalyst powders, which are not detectable for BET analysis, however, XRD can detect the sub-grains within particles (Fu *et al* 2009). Thus by calculating degree of agglomeration (d/D_{XRD}), the extent of agglomeration was ascribed to increase in the case of Cu/TiO_2 catalyst.

3.1.2 X-ray diffraction results

The crystallinity of the prepared samples was examined by XRD analysis. A single anatase phase TiO_2 was formed for all TiO_2 catalysts. The peaks at 2θ values of 25.3, 30.8, 37.8, 48.1, 53.9, 54.3, 56.6, 70.2 and 75.1, 82.7 were identified by comparing with literature data and confirm that the particles are polycrystalline with an anatase structure (Rouquerol & Rouquerol 1999). All peaks are in good agreement with the standard spectrum (JCPDS no 01-075-2246).

The enrichment of the surfaces by metal species, not detected by X-ray diffraction, indicates an imperfect diffusion of metal ions into the support at the low temperature of calcinations to which the samples were subjected. This is also confirmed by Di Paola *et al.* (2004) the decrease of the specific surface areas with increasing the metal loading that can be justified by the obstruction of the pores of the support by metal oxides. However, the relative intensities of the anatase peak vary among samples. High TiO_2 crystallinity was obtained with the addition of 0.5wt% Cu^{+2}. The TiO_2 without Cu^{2+} produced relatively small diffraction peaks of anatase at 25°, in contrast to the patterns of the samples with Cu^{2+}. Therefore, phase transformation was not fully achieved without Cu^{2+}, as the TiO_2 retained portions of the inactive amorphous phase.

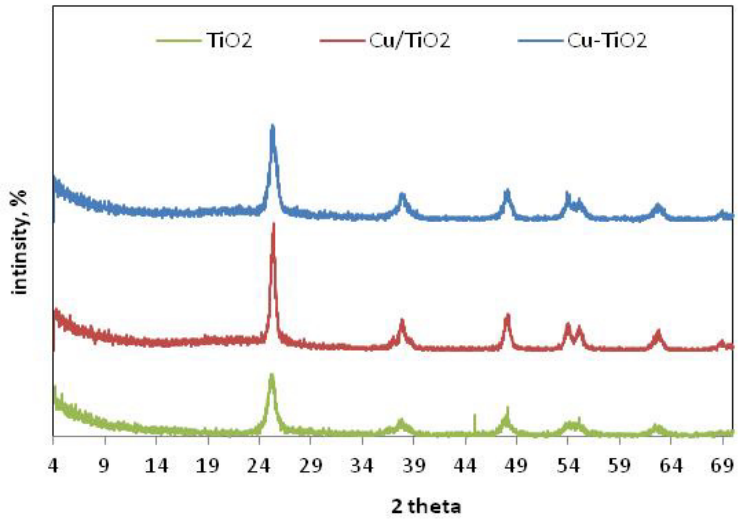

Figure 2. XRD of TiO_2 catalysts

3.1.3 Raman spectra

Figure 4. Shows a summary of Raman spectra of TiO_2 catalysts. Structure of TiO_2 is confirmed in the FTIR spectrum. The peak of TiO_2 anatase observed ca. 400- 700 cm^{-1} (Ti–O vibration) was observed in both irradiated and non-irradiated TiO_2. The two bands appearing at 1525 and 1644 cm^{-1}, in all spectra are attributed to surface-adsorbed water and the bending mode of hydroxyl groups.

Bands observed ca. 3660 and 3740 cm^{-1} are characterized to isolated OH-groups vibrations in the case of the anatase structure (Jackson, G. Parfitt 1976).

For Cu-TiO_2 the broad peaks at 3448 cm^{-1} and the peaks at 1644 cm^{-1} are characteristic of the H–O bending mode of hydroxyl groups present on the surface due to moisture. These are crucial to the photocatalytic reactions since they can react with photoexcited holes generated on the catalyst surface and produce hydroxyl radicals (Ding et al. 2000), which are powerful oxidant. Also Poliah & Sreekantan (2011) reported that the higher surface acidity led to a higher degree of adsorption of the OH radicals increase band intensity at 1640 cm^{-1}.

However; the high level of anatase hydration is probably also responsible for broad absorption bands in the spectral range of 1023 cm^{-1} in Cu-TiO_2 catalyst. The signals of copper are not observed in the case of IR.

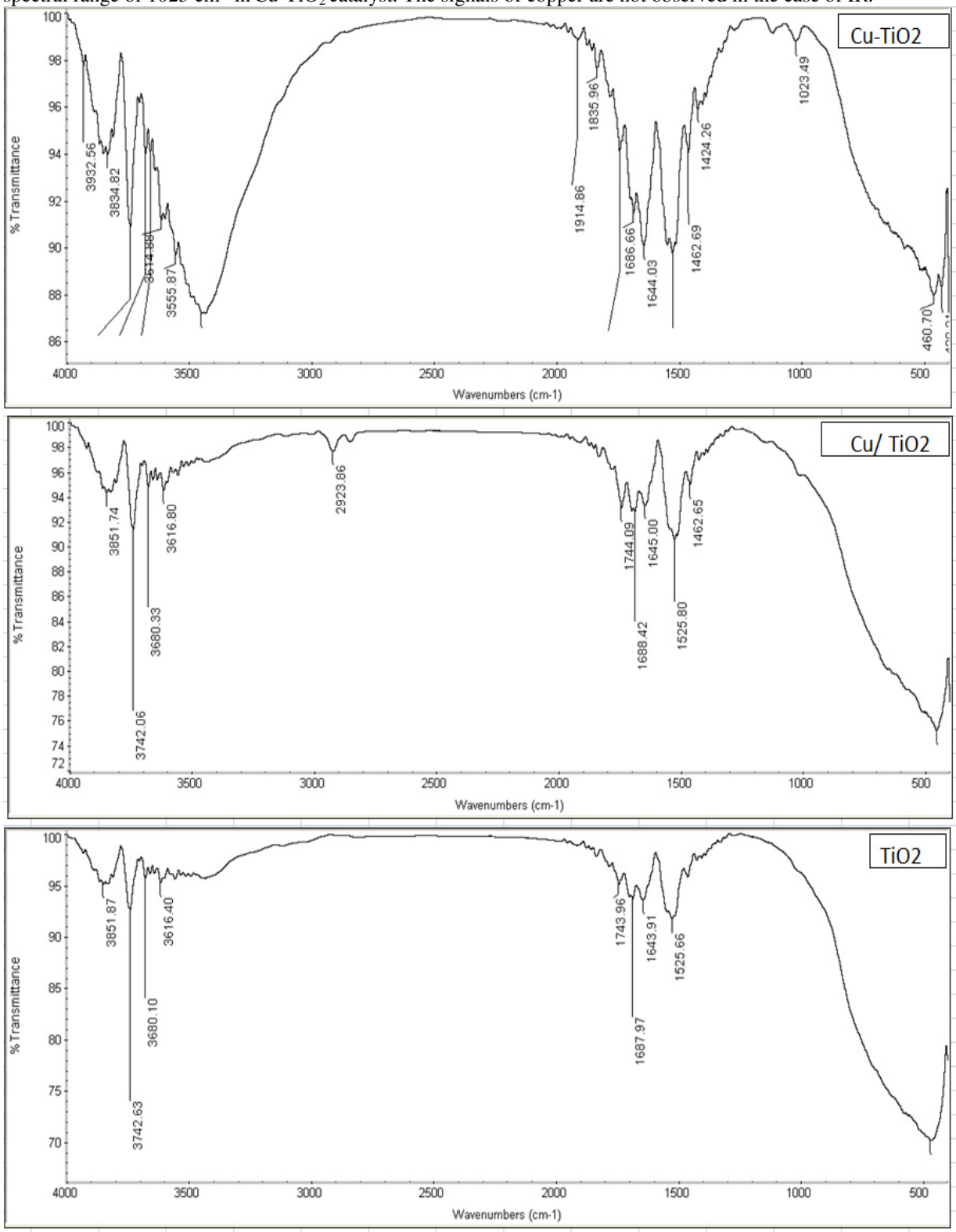

Figure 4. FTIR of TiO_2 Catalysts

3.1.4 High Resolution Transmission Electron Microscopy (HRTEM)

The TEM images of TiO_2 and Cu/TiO_2 samples are shown in Figure 5. They showed regular round shaped particles. The samples have slightly collapsed spherical bi-continuous structure. There was no significant

difference between Cu^{+2} and Ti^{+4} particles. For Cu-TiO_2 the lattice distance was measured to be 0.27 nm according to the HRTEM image, which could be assigned to the lattice face of Cu_2O (1 1 1). The nanocrystallites size of 19.6, 11.75 and 20.6 nm respectively.

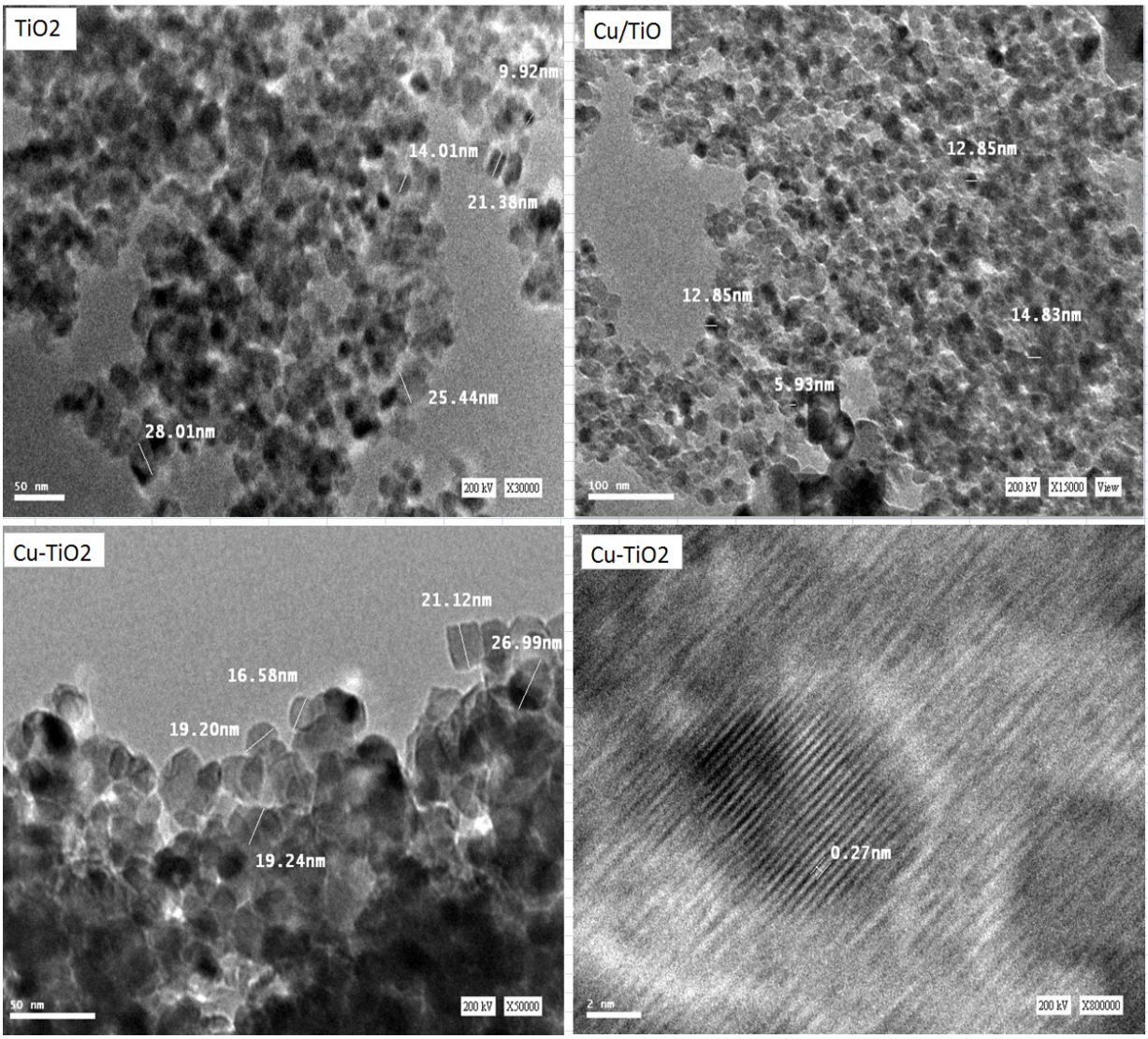

Figure 5. TEM image of TiO_2 Catalysts

3.2 Photocatalytic 4-NP degradation results

4-NP, known to be a very stable and refractory pollutant in industrial wastewater, was used as a probe organic compound to evaluate the photocatalytic performance of various catalysts (Di Paola et al. 2003) 4-NP degradation is negligible under simulated UV irradiation in the absence of catalyst due to the stable structure of 4-NP.

As shown in Figure 6, among all the catalysts, Cu-TiO_2 sample shows the highest photocatalytic activity, with the 4-NP concentration reduced as much as 70% in 150 min. whereas; it reduced as much as 37% and 53% in 150 min for TiO_2 and Cu/TiO_2 catalysts respectively.

It is important to note that the TiO_2 sample displays much lower activity despite the large surface area about 127m^2/g may be due to its imperfect crystallization from the XRD pattern (Figure 2) is considered to increase the probability of the mutual e^-/h^+ recombination at both surface and bulk traps. Beside the low acidity of TiO_2 (Table 1) led to a lower degree of adsorption of the OH radicals as shown from FTIR spectra.

For Cu-TiO_2 sample prepared by co-precipitation displays a higher activity than that of Cu/TiO_2. Therefore, it is believed that the large close interface between the two semiconductors plays a pivotal role to the excellent photocatalytic performance of Cu-TiO_2 sample. However, the total pore volume of Cu-TiO_2 catalyst amount to 0.476 cm^3g^{-1}. This affected postively on the diffusion of PNP throgh catalyst pores.

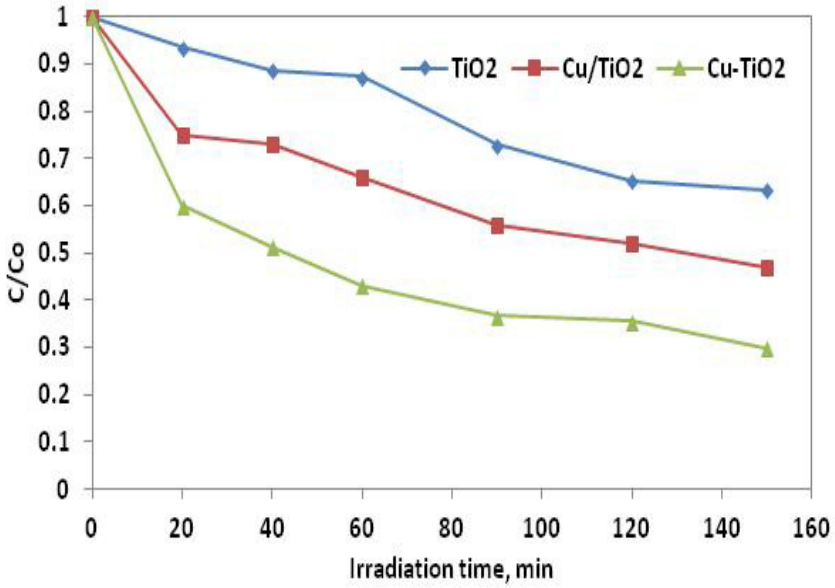

Figure 6. 4-NP concentration vs. irradiation time using different photocatalysts under UV irradiation

It is well known that TOC is an important evaluation criterion for the mineralization of organic pollutant. The reduction of TOC are 24% , 45% and 46% after photodegradation of 4-NP for 150 min over TiO_2, Cu/TiO_2 and Cu-TiO_2 catalysts. The mineralization rate far below the decolorization rate indicates the formation of some organic intermediates during the photocatalytic process.

For a better understanding of photocatalytic efficiency of the above catalysts, the kinetic analysis for the photodegradation of 4-NP is investigated (Figure 7). It is seen that all the degradation processes follow a pseudo first-order kinetics equation:

$$\ln(C_o/C_t) = kt$$

where k is the apparent rate constant of the degradation. The k value of Cu-TiO_2 (0.005 min^{-1}) is 1.5 and 1.3 times as great as that of TiO_2 (0.0033 min^{-1}) and Cu/TiO_2 (0.0038 min^{-1}) although its surface area (60 m^2g^{-1}) is much smaller than that of TiO_2 (127 $m^2 g^{-1}$) and Cu/TiO_2 (116 m^2g^{-1}). In general, the introduction of transition metals resulted in the change of the electronic environment of TiO_2. Based on the TEM results, for Cu-TiO_2, Cu metals were adsorbed on the surface of TiO_2 as little island of metal particle that acts as the active sites of the photocatalytic reaction and may favor separating charge carriers efficiently, inhibiting the recombination of electron–hole pairs, and ultimately causing the enhancement of the reactivity (Elsalamony & Mahmoud 2012). The half life time ($t_{1/2}$) is related to the degradation (k) by the following equation:

$$t_{\frac{1}{2}} = \frac{\ln(2)}{k}$$

The time taken for 50% degradation of a nitrophenol is 210.04 min, 182.41 min and 138.6 min using TiO_2, Cu/TiO_2 and Cu-TiO_2 catalysts TiO_2, Cu/TiO_2 and Cu-TiO_2 catalysts respectively.

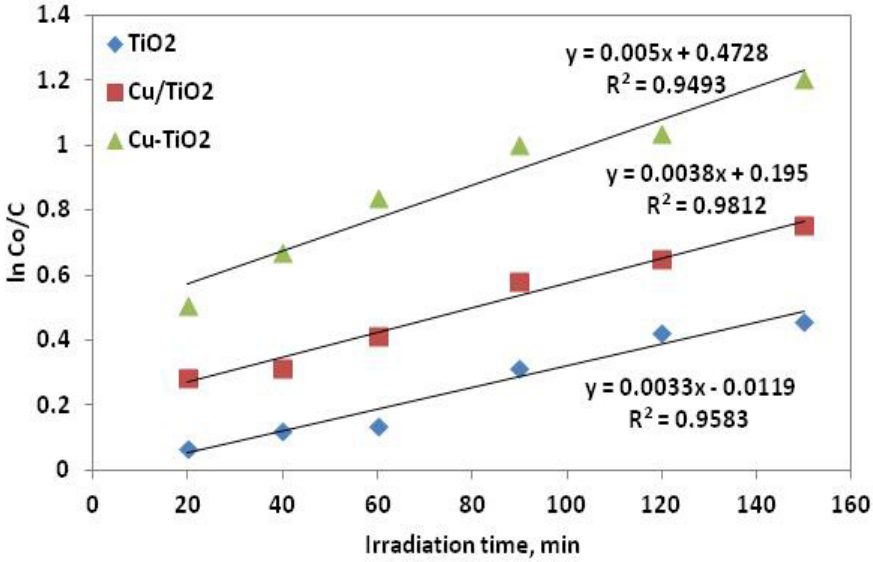

Figure 7. The apparent first-order kinetics for the photocatalysts

3.2.1 Effect of concentration of NP

Different concentration gradients, 10, 20, 30, 40 and 50 mg L^{-1}, were chosen to analyze the effect of varying initial NP concentration on the degradation efficiency, as shown in Figure 8. It is clearly seen that the NP degradation rate decreased when its initial concentration increased. This result was consistent with the studies of others (Wang *et al.* 2008; Xiao *et al.* 2012).

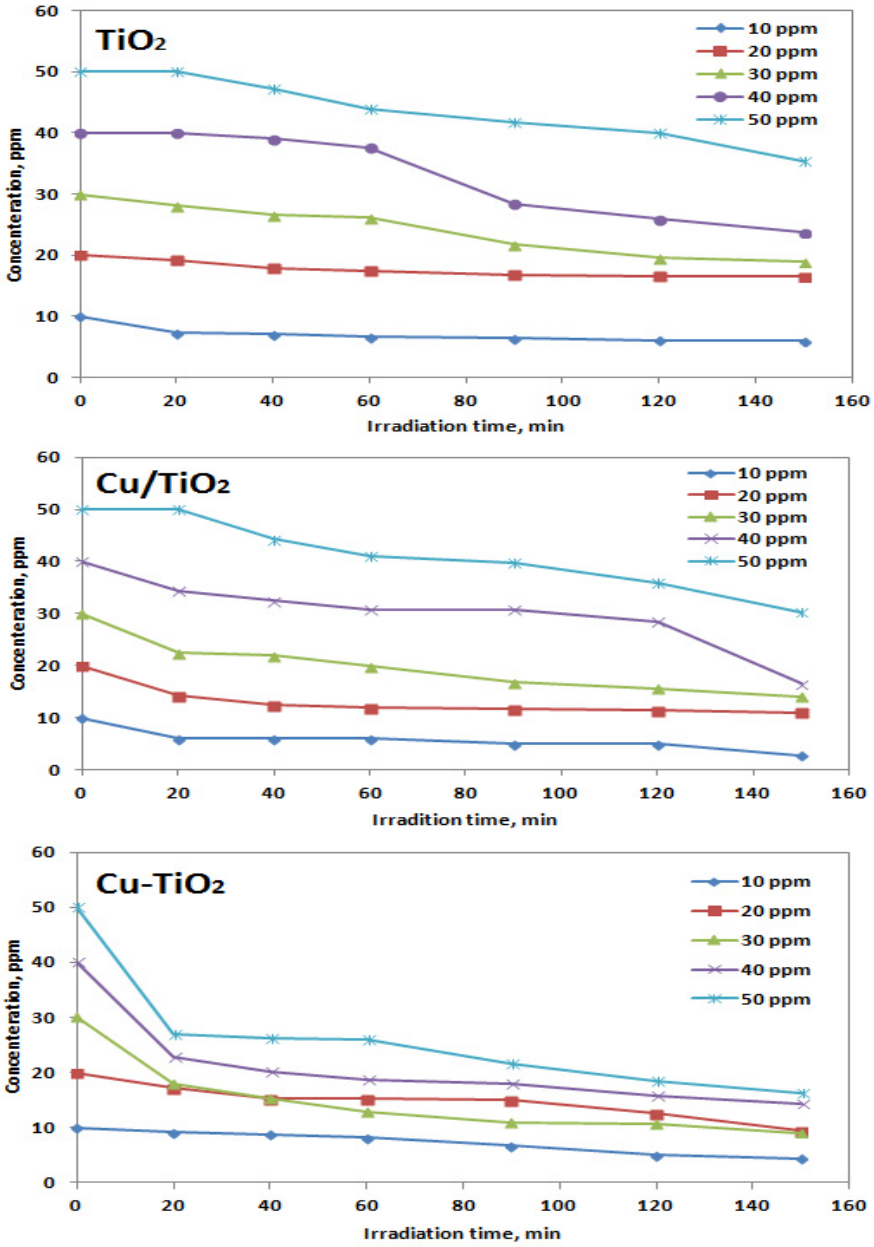

Figure 8. Effect of initial NP concentrations on photocatalytic degradation process using photocatalysts under UV irradiation.

An explanation was that as the initial NP concentration increased, more and more pollutant molecules and intermediate products were accumulated on the surface of photocatalysts, thus the generation of reactive oxygen species was reduced because of the inhibited adsorption of incident photons for the active sites, finally causing the depressed photocatalytic activity.

4. Conclusion

In summary, the Cu-TiO_2 prepared by co-preceptation method showed high catalytic abilities during PNP degradation under a UV lamp. This activity is attributed to its large total pore volume as well as its high acidity and maintaining a good control of the particle agglomeration. Also, FTIR spectra show two strong bands characteristic of the H–O bending mode of hydroxyl groups present on the surface of catalyst due to moisture. These are crucial to the photocatalytic reactions since they can react with photo-excited holes generated on the catalyst surface and produce hydroxyl radicals which are powerful oxidant. A TOC removal of ca. 46% was

achieved and half time 138 min. Therefore, it is believed that the large close interface between the two semiconductors plays a pivotal role to the excellent photocatalytic performance of Cu-TiO_2 catalyst.

References

Adán, C., Bahamonde, A., Fernández-García, M., Martínez-Arias, A. (2007). Structure and activity of nanosized iron-doped anatase TiO_2 catalysts for phenol photocatalytic degradation, *Appl. Catal. B,* 72, 11-17. http://dx.doi.org/10.1016/j.apcatb.2006.09.018

Anpo, M., Tackeuchi, M. (2003). The design and development of highly reactive titanium oxide photocatalysts operating under visible light irradiation. *J. Catal.*, 21, 505-516. http://dx.doi.org/10.1016/S0021-9517(02)00104-5

Augugliaro, V., Litter, M., Palmisano, L., Soria, J. (2006). The combination of heterogeneous photocatalysis with chemical and physical operations: A tool for improving the photoprocess performance, *J. Photochem. Photobiol.* C 7, 127-144. http://dx.doi.org/10.1016/j.jphotochemrev.2006.12.001

Bo, L. L., Quan, X., Chen, S., Zhao, H.M., Zhao, Y.Z. (2006). Degradation of *p*-nitrophenol in aqueous solution by microwave assisted oxidation process through a granular activated carbon fixed bed. *Water Res.*, 40, 3061–3068, http://dx.doi.org/10.1016/j.watres.2006.06.030

Cao, Y.B., Fan, J.M., Bai, L.Y., Yuan, F.L., Chen, Y. F. (2010). Morphology Evolution of Cu_2O from Octahedra to Hollow Structures. *Cryst. Growth Des.,* 10, 232–236. doi: 10.1021/cg9008637

Chen, J.-W., Shi, J.-W., Wang, X., Ai, H.-Y., Cui, H.-J., Fu, M.-L. (2013). Hybrid metal oxides quantum dots/TiO_2 block composites: Facile synthesis and photocatalysis application. *Powder Technology,* 246, 108-116, http://dx.doi.org/10.1016/j.powtec.2013.05.014

Di Paola, A., Augugliaro, V., Palmisano, L., Pantaleo, G., Savinov, E. (2003). Heterogeneous photocatalytic degradation of nitrophenols. *J. Photochem. Photobiol. A*, 155, 207-214. doi. S1010-6030(02)00390-8.

Di Paola, A., García-López, E., Marcí, G., Martín, C., Palmisano, L., Rives, V., Venezia, A. M. (2004). Surface characterization of metal ions loaded TiO_2 photocatalysts: structure–activity relationship. *Appl. Cata. B: Envir.,* l 48, 223–233. http://dx.doi.org/10.1016/j.apcatb.2003.10.015

Ding, Z., Lu, G.Q., Greenfield, P.F. (2000). Role of the crystallite phase of TiO_2 in heterogenous photocatalysis for phenol oxidation in water. *J. Phys. Chem. B,* 104, 4815–4820. doi. 10.1021/jp993819b.

Dobrosz-Gómeza, I., Gómez Garcíaa, M.A., Szynkowskab, M.I., Kocembab, I., Rynkowski, J.M. (2012). Surface, structural and morphological characterization of nanocrystalline ceria–zirconia mixed oxides upon thermal aging. *Cata. Today*, 191, 142-145, http://dx.doi.org/10.1016/j.cattod.2011.12.031

Elsalamony, R. A. & Mahmoud, S. A. (2012). Preparation of nanostructured ruthenium doped titania for the photocatalytic degradation of 2-chlorophenol under visible light. *Arabian Journal of Chemistry*, in press. http://dx.doi.org/10.1016/j.arabjc.2012.06.008.

Farbod, M., Kajbafvala, M. (2013). Effect of nanoparticle surface modification on the adsorption-enhanced photocatalysis of Gd/TiO_2 nanocomposite. *Powder Technology,* 239, 434-440. http://dx.doi.org/10.1016/j.powtec.2013.02.027

Fu, Y.-P., Hu, S.-H., Liu, B.-L. (2009). Structure characterization and mechanical properties of CeO_2–ZrO_2 solid solution system. *Ceramics International*, 35, 3005–3011. http://dx.doi.org/10.1016/j.ceramint.2009.04.001

Fuentes, R. O., Woollins, J. D., Baker, R. T. (2010). Temperature effects on structural properties in the synthesis of nanocrystalline $Zr_{0.5}Ce_{0.5}O_2$solid solution: A study by XRD and HRTEM. *J. Alloys and Compounds,* 495, 565–569. http://dx.doi.org/10.1016/j.jallcom.2009.11.080

Jackson, P., Parfitt, G. (1971). Infra-red study of the surface properties of rutile: Water and surface hydroxyl species, Trans. Farad. Soc., 67, 2469- 2483. **doi:** 10.1039/TF9716702469

Khalid, N.R., Ahmed, E., Hong, Z., Ahmad, M., Zhang, Y., Khalid, S. (2013). Cu-doped TiO_2 nanoparticles/graphene composites for efficient visible-light photocatalysis. *Ceramics International*, 39, 7107-7113, http://dx.doi.org/10.1016/j.ceramint.2013.02.051

Khanna, A., Shetty, V. K. (2014). Solar light induced photocatalytic degradation of Reactive Blue 220 (RB-220) dye with highly efficient $Ag@TiO_2$ core–shell nanoparticles: A comparison with UV photocatalysis. *Solar Energy*, 99, 67-76. http://dx.doi.org/10.1016/j.solener.2013.10.032

Kuo, C.H., Huang, M.H. (2008). Facile synthesis of Cu_2O nanocrystals with systematic shape evolution from cubic to octahedral structures. *J. Phys. Chem. C,* 112, 18355–18360. doi**:** 10.1021/jp8060027

Litter, M., Navío, J.A. (1996). Photocatalytic properties of iron-doped titania semiconductors, *J. Photochem. Photobiol. A* , 98, 171-181. http://dx.doi.org/10.1016/1010-6030(96)04343-2

M. Schiavello, M. (1988). (Ed.), Photocatalysis and Environment: Trends and Applications, Kluwer Academic Publishers, Dordrecht.

Malato, S., Fernández-Ibánez, P., Maldonado, M.I., Blanco, J., Gernjak, W. (2009). Decontamination and disinfection of water by solar photocatalysis: Recent overview and trends, *Catal. Today,* 147, 1-59. http://dx.doi.org/10.1016/j.cattod.2009.06.018

Palmisano, L., Sclafani, A. in: Schiavello, M. (1997). (Ed.), Heterogeneous Photocatalysis, Wiley Series in Photoscience and Photoengineering, vol. 3, Wiley, Chichester, Chapter 4, p. 109 and references therein.

Pelizzetti, E., Serpone, N. (1986) (Eds.), Homogeneous and Heterogeneous Photocatalysis, Reidel, Dordrecht.

Pelizzetti, E., Serpone, N. (1989) (Eds.), Photocatalysis: Fundamental and Applications, Wiley, New York.

Poliah, R. & Sreekantan, S. (2011). Characterization and Photocatalytic Activity of Enhanced Copper-Silica-Loaded Titania Prepared via HydrothermalMethod. *J. Nanomaterials*, 1-5. doi. 10.1155/2011/239289.

Quiroz, M.A., Reyna, S., Martinez-Huitle, C.A., Ferro, S., De-Batteisti, A. (2005). Electrocatalytic oxidation of *p*-nitrophenol from aqueous solutions at Pb/PbO_2 anodes. *Appl. Catal.B: Environ.,* 59, 259–266. http://dx.doi.org/10.1016/j.apcatb.2005.02.009

Ravikovitch, A.V. Neimark, P.I. (2002). Density Functional Theory of Adsorption in Spherical Cavities and Pore Size Characterization of Templated Nanoporous Silicas with Cubic and Three-Dimensional Hexagonal Structures. Langmuir 18, 1550-1560. doi. 10.1021/la0107594

Rouquerol, F., Rouquerol, J., Sing, K. (1999). Adsorption by Powders and Porous Solids: Principles, Methodology and Applications. Academic Press, San Diego.

Somasundaram, S., Chenthamarakshan, C.R.N., Tacconi, N.R., Rajeshwar, K. (2007). Photocatalytic production of hydrogen from electrodeposited p-CuO_2 film and sacrificial electron donors*, Int. J. Hydrogen Energy*, 32, 4661–4669. http://dx.doi.org/10.1016/j.ijhydene.2007.06.028

Su, B.Q., Ma, Y.J., Du, Y.L., Wang, C.M. (2009). Study of photoelectrocatalytic degradation behavior of *p*-nitrophenol with nano-TiO_2 modified film at a rotating ring–disk electrode, *Electrochem. Commun.*, 11, 1154–1157. http://dx.doi.org/10.1016/j.elecom.2009.03.035

Wang, C. C., Lee, C. K., Lyu, M. D., Juang, L. C. (2008). Photocatalytic degradation of C.I. Basic Violet 10 using TiO_2 catalysts supported by Y zeolite: An investigation of the effects of operational parameters. *Dyes and Pigments*, 76, 817–824. http://dx.doi.org/10.1016/j.dyepig.2007.02.004.

Xiao, X., Hao, R., Zuo, X. X., Nan, J. M., Li, L.S., Zhang, W.D. (2012). Microwave-assisted synthesis of hierarchical $Bi_7O_9I_3$ microsheets for efficient photocatalytic degradation of bisphenol-A under visible light irradiation. *Chem. Eng. J.* 209, 293–300. http://dx.doi.org/10.1016/j.cej.2012.07.142.

Yu, S.Q., Hu, J., Wang, J. L. (2010). Radiation-induced catalytic degradation of p-nitrophenol (PNP) in the presence of TiO_2 nanoparticles, *Radiat. Phys. Chem,* 79, 1039–1046. http://dx.doi.org/10.1016/j.radphyschem.2010.05.008

Zhiyu, W., Haifeng, C., Peisong, T., Weiping, M., Fuan, Z., Guodong, Q., Xianping, F. (2006). Hydrothermal in situ preparation of the copper phthalocyanine tetrasulfonate modified titanium dioxide photocatalyst , *Colloids and Surfaces A: Physicochem. Eng. Aspects,* 289, 207–211. http://dx.doi.org/10.1016/j.colsurfa.2006.04.049